Diaphanous-1 Affects the Nanoscale Clustering and Lateral Diffusion of Receptor for Advanced Glycation Endproducts (RAGE)

Qiaochu Zhu,[1] Emily A. Smith[1*]

[1]*Department of Chemistry, Iowa State University, Ames, IA 50011, United States*

ABSTRACT The interactions between the cytoplasmic protein diaphanous-1 (Diaph1) and the receptor for advanced glycation endproducts (RAGE) drive the negative consequences of RAGE signaling in several disease processes. Reported in this work is how Diaph1 affects the nanoscale clustering and diffusion of RAGE measured using super-resolution stochastic optical reconstruction microscopy (STORM) and single particle tracking (SPT). Altering the Diaph1 binding site has a different impact on RAGE diffusion compared to when Diaph1 expression is reduced in HEK 293 cells. In cells with reduced Diaph1 expression (RAGE-Diaph1$^{-/-}$), the average RAGE diffusion coefficient is increased by 35 %. RAGE diffusion is known to be influenced by the dynamics of the actin cytoskeleton, and actin labeling shows reduced Diaph1 expression results in cells with reduced filopodia density and length. In contrast, when two RAGE amino acids that interact with Diaph1 are mutated (RAGE$_{RQ/AA}$), the average RAGE diffusion coefficient is decreased by 16 %. Since RAGE diffusion is slowed when the interaction between Diaph1 and RAGE is disrupted, the interaction of the two proteins results in faster RAGE diffusion. In both RAGE$_{RQ/AA}$ and RAGE-Diaph1$^{-/-}$ cells the number and size of RAGE clusters is decreased compared to cells expressing RAGE and native concentrations of Diaph1. This work shows that Diaph1 has a role in affecting RAGE clusters and diffusion.

Keywords: Super-resolution stochastic optical reconstruction microscopy, Single particle tracking, Receptor clusters, Receptor diffusion

1. Introduction

The receptor for advanced glycation endproducts (RAGE) is a member of the immunoglobulin superfamily of cell surface proteins [1, 2], and has been implicated in the negative consequences of numerous chronic diseases based on evidence from human and animal studies [3-5]. RAGE exhibits promiscuous binding with multiple ligands, including S100/calgranulins [4, 6], advanced glycation endproducts [3], high mobility group box 1 [7], amyloid A or β peptide [8, 9], and Mac-1/β2 integrin [10]. Interactions between RAGE and its ligands are abnormally regulated in Alzheimer's disease, Parkinson's disease, diabetic neuropathy, inflammatory disease, and cardiovascular disease [11]. In addition, the elevated levels of RAGE ligands that may be present as a consequence of these diseases results in RAGE upregulation [12]. RAGE may be a good biomarker for many human diseases, and is also a potential therapeutic target [13]. There are, however, many missing details about the mechanisms that govern the biophysical properties of this important receptor.

RAGE consists of three extracellular domains, a transmembrane helix, and a short cytoplasmic tail. The V-type and C1-type extracellular domains are involved in ligand binding, while the C2 extracellular domain supports the rigid V-type/C1-type tandem domain. Ligand binding to the extracellular domain of RAGE initiates signal transduction [14, 15]. Downstream signaling includes phosphorylation of mitogen-activated protein kinase (MAPK), phosphatidylinositol 3-kinase (PI3K/Akt), Rho GTPases (Rac-1 and Cdc42) and activation of nuclear factor kappa B (NF- κB) [16-18]. Several of the RAGE ligands are multivalent, including the S100/calgranulins (S100B, S100A12). The multivalent binding drives RAGE clusters on the cell surface [6], which is an important aspect of downstream signal transduction [15, 16, 19, 20]. Changes in the size of RAGE clusters may affect the recruitment of Diaph1 and subsequent signal transduction pathways [21]. Based on data for a

soluble variant of RAGE, Xie et al. proposed that full-length RAGE on the plasma membrane of HEK293T cells may form homooligomers, which would be nanoscale in size (i.e., below the diffraction limit of an optical microscope) [14].

RAGE signal transduction is a consequence of the interaction between the formin homology 1 (FH1) domain of diaphanous-1 (Diaph1) with the RAGE cytoplasmic tail [22-24]. Two amino acids, Arginine-5 (R5) and Glutamine-6 (Q6), of the RAGE cytoplasmic tail are essential for interactions with Diaph1 based on the lack of binding for a R5A/Q6A RAGE mutant [25]. When Diaph1 expression is reduced via RNA interference, RAGE singling through Akt is blocked and the migration of SMC cells is suppressed [22, 26]. Diaph1 plays an essential role in regulating a variety of cytoskeleton-dependent cellular processes under stimulation including actin and microtubule polymerization as well as the formation of filopodia for vesicle trafficking [27-31] Under non-stimulating conditions, Diaph1 controls cellular adhesion by stabilizing microtubules for localized clustering of integrin-β1 at the plasma membrane [32].

Although the cytoplasmic interactions between RAGE with Diaph1and the resulting signaling pathways have been studied, the effect of Diaph1 on RAGE diffusion and nanoscale clusters remains unknown. These properties can affect biomolecular interactions, signal transduction and overall cellular function [33-35]. In order to provide this missing information, single particle tracking (SPT) is used to individually track the diffusion of a subset of diffusely-labeled receptors and to test the role of Diaph1 in affecting RAGE diffusion. In addition, the size of RAGE nanoscale clusters is measured using super-resolution stochastic optical reconstruction microscopy (STORM). Disrupting the interaction between RAGE and Diaph1 through protein mutation results in different RAGE clustering

and diffusion properties compared to when Diaph1 expression is reduced altogether. The latter may be the result of disrupting the actin cytoskeleton when Diaph1 expression is reduced. This conclusion is supported by previous reports where we show that RAGE diffusion is altered by compounds that inhibit actin depolymerization [36].

2. Materials and methods

2.1 Cell culture, actin staining, and filopodia quantification

Details of RAGE plasmid construction, down-regulation of Diaph1, Western blotting and RT-PCR methods are provided in the supplementary material. Cells were plated onto an 8-well Nunc™ Lab-Tek™ chambered glass slide. For intracellular actin staining in HEK293 cells, cells were fixed with 4% paraformaldehyde (Sigma Aldrich) in PBS for 30 min at room temperature after rinsing cells with phosphate buffered saline (PBS) three times. Cells were washed twice with 1 mg/mL sodium borohydride (Fisher Chemical) in PBS for 5 min to quench cellular autofluorescence. The cells were permeabilized with 0.1% Triton-X100 (Thermo Scientific) in PBS for 5 min, and the actin filaments were stained using Alexa Fluor 488 phalloidin (1:100) (Invitrogen™) in PBS for 30 min. After rinsing the cells with PBS, they were imaged by using a Leica TCS SP5 confocal microscope with a 100×-magnification 1.4-NA oil-immersion objective. Images were collected with a frame rate of 200 Hz and 400 nm z-step size. The ImageJ plugin FiloQuant was used to quantify the filopodia length and density [37, 38]. The filopodia density is defined as the ratio of the number of filopodia per a given length of the cell edge.

2.2 STORM and clusters analysis

An 8-well Nunc™ Lab-Tek™ chambered glass slide was sonicated in 1M KOH for 15 min then rinsed with deionized water. The glass slide was coated with 0.01% poly-l-lysine

solution then washed with deionized water and dried under ultraviolet radiation. Cells were subcultured onto the glass slide until 60% confluence was achieved. The cells were washed with PBS twice then fixed with 1% paraformaldehyde for 10 min at room temperature. After three PBS washes, the cells were incubated with anti-RAGE antibody (1:100) in incubation buffer (5% normal goat serum (Invitrogen^{TM}) and 1% BSA prepared in PBS solution) for 1h at room temperature. The RAGE primary antibody interacts with the extracellular domain of RAGE. The cells were washed with incubation buffer three times and then incubated with Alexa Fluor 647 F(ab')2-Goat anti-rabbit (A21246, Invitrogen^{TM}) (1:1000) for 30 min at room temperature. After three PBS washes, 800 µL of imaging buffer (50 mM NaCl, 10% glucose, 0.5 mg/mL glucose oxidase, 40 µg/mL catalase, and 50 mM cysteamine in 10 mM Tris, pH = 8.0) were added into each well then covered by a glass coverslip. The labeling conditions used in this study ensure that the signal is coming only from receptor in the membrane. No detectable labeling was measured for HEK293 cells that lack the expression of exogenous RAGE. For STORM experiments, a Nikon TE2000U epifluorescence/TIRF microscope equipped with a 100× 1.49 NA oil immersion objective and a 635-nm excitation laser (LQC635, CW laser diode, Newport) with a power density of 1.5 KW/cm^2 were used. Movies were collected with 15,000 frames, a 40 ms exposure time, and a 64×64 frame size using a EMCCD (Andor iXon^{EM}+ DU-897). The ImageJ plugin ThunderSTORM was used to localize single molecules in each frame of the movie and to construction super resolution images [39]. Briefly, the size of each pixel (0.16 µm/pixel), photoelectrons per A/D count EM gain (600), exposure time (40 ms) were used as inputs for the camera settings. Single molecules were localized using weighted least-squares fitting of an integrated Gaussian PSF enabled to detect up to two single molecules within a diffraction-limited area. The localization precision and Ripley's K analysis were performed using LocAlization Microscopy Analyzer (LAMA) [40].

2.3 Single particle tracking

Cells were subcultured onto 8-well Nunc™ Lab-Tek™ chambered glass slides that were coated with 0.01% poly-L-lysine solution (P4704, Sigma Aldrich) for 48 h. The medium was changed to 3% BSA in DMEM for 18 h to coat any remaining glass surface. The anti-HA labeled QDs (AHA-QDs) were prepared as previously published [41]. After 100 pM AHA-QDs were diluted in imaging buffer (20 μM HEPES, 6 μM D-glucose, 0.3 μM Na_2HPO_4, 138 μM NaCl, 4 μM $NaHCO_3$, 0.4 μM KH_2PO_4, 5 μM KCl, 0.4 μM $MgSO_4 \cdot 7H_2O$, 0.5 μM $MgCl_2 \cdot 6H_2O$, 1 μM $CaCl_2$) with 0.1% BSA, cells were incubated with AHA-QDs for 15 min at 37 °C. This labeling method is highly specific to cells expressing RAGE. In Fig. S1, there is an average of 2 ± 1 QDs per wild-type HEK293 cell that does not have detectable levels of RAGE as measured by Western blot analysis. The QDs measured in wild-type HEK293 cells exhibit no movement within the uncertainty of the localization measurement, and have an average diffusion coefficient less than 0.0018 $\mu m^2/s$. In cells expressing transgenic RAGE, an average of 20 ± 10 QDs per cell is bound to the cell (Fig. S1). In order prevent skewing the SPT results with signals that may correspond to QDs not bound to RAGE (nonspecific binding), only trajectories that result in a RAGE diffusion coefficient larger than 0.0018 μm/s were considered.

Cells were washed with imaging buffer before performing microscopy experiments. SPT experiments were performed at 37 °C with an Eclipse Nikon (TE2000U) microscope in wide-field, epi-mode with a 100× 1.4 NA oil-immersion objective. The light from a mercury lamp was passed through a filter set (excitation: 425/25 nm; emission: 605/20 nm; Omega Optical. The signal was collected by an Andor iXon^{EM}+ DU-897 back-illuminated electron-multiplying charge coupled device (EMCCD) with a 40 ms acquisition time and 700 frames

were collected. A 2D/3D single-particle tracking plug-in (MosaicSuite) for ImageJ was used to track single particles in each frame over time to generate trajectories of x-y location [41-43].

More than 150 single particle trajectories from at least 20 cells were collected for each cell line, and were subsequently analyzed using TrackArt, which is a MATLAB application based on a previously described algorithm [44, 45]. To quantify RAGE diffusion on the ensemble level, the mean square displacement (MSD, r^2) was determined by the cumulative probability distribution (CPD) of the square displacement over consecutive time lags (4s). This method has been extensively used to quantify the diffusion coefficient and fractional populations in multiple system [46-49]. CPD is defined as the probability that a particle remains within a circle with a radius r. The fraction (f) of each population can be separately estimated. A single population exhibiting Brownian motion yields a single exponential model (1p model) and can be fit by:

$$CPD(r^2, t) = 1 - \exp(-\frac{r^2}{4Dt})$$

where D is the diffusion coefficient. The goodness-of-fit was determined by calculating the residual sum of squares. If a single exponential model failed to accurately fit the data, then a double exponential model (2p model) was used:

$$CPD(r^2, t) = 1 - \langle f \exp\left(-\frac{r^2}{4D_f t}\right) + (1 - f) \exp\left(-\frac{r^2}{4D_s t}\right)\rangle$$

The 2p model produces two diffusion coefficients: D_f for the fast population and D_s for the slow population. The fit results also provide the relative fractions f and 1 – f for the fast population and slow population, respectively [50].

The MATLAB APM_GUI based on an algorithm developed by Simson and Menchon [51, 52] was used to detect confined motion within each trajectory. Confined motion is defined as diffusive motion that is restricted by boundaries that cannot be crossed [53]. Within the confinement boundaries, Brownian diffusion may occur. Briefly, all trajectories were categorized as either Brownian motion or non-random (i.e., confined) motion based on the probability (L) of staying within a region of radius R. The critical confinement index (L_c) and critical confinement time (t_c) were obtained from simulated Brownian trajectories for a range of diffusion coefficients as previously described [41]. A trajectory with $L_c > 3.16$ and $t_c > 1.95$ is categorized as confined motion. If a trajectory exhibits confined motion, the diffusion coefficient inside confined domains (D_{in}), the size of the confined domain (R), and the time in the confined domain (t) were calculated.

2.4 Statistical analysis

The reported data was determined to exhibit a parametric distribution or non-parametric distribution using the Shapiro-Wilk Test to test for normality. The statistical significance of all parametric distributions was calculated using the F-test at the 95% confidence level and then a paired/unpaired (as determined by the F-test) Student's t-test with a two-tailed distribution. The statistical significance of all non-parametric distributions was calculated using the Mann-Whitney test with a two-tailed distribution. All resulting p-values below 0.05 are reported in the figures. (If a p-value was not reported, its value was greater than 0.05), unless otherwise noted in the figure legend.

3. Results and discussion

3.1 RAGE forms nanoscale clusters that are altered when Diaph1 expression is reduced or when the interaction between Diaph1 and RAGE is altered

To measure RAGE clusters and diffusion under conditions of altered interaction with Diaph1, stably transfected HEK 293 cells were developed that expressed RAGE or RAGE with a R5A/Q6A mutation on the cytoplasmic tail ($RAGE_{RQ/AA}$). The amino acid sequence in the transmembrane domain and intracellular domain of RAGE and $RAGE_{RQ/AA}$ are shown in Fig. S2a. An HA epitope was added to the extracellular domain of all RAGE sequences to facilitate specific labeling with an HA antibody. It has been shown that the cell signaling measured by phosphorylation of ERK is not altered in cells expressing RAGE with and without the HA epitope [41].

Diffraction-limited wide-field fluorescence images show a fairly uniform RAGE distribution throughout the cell membrane with a higher signal around the periphery of the cell (Fig.1a). STORM allows the RAGE distribution to be measured with 21-nm localization precision as determined by nearest-neighbor-based analysis. In Fig.1b and Fig.1c, RAGE clusters of varying size are observed; clusters are also measured for cells expressing $RAGE_{RQ/AA}$ (Fig.S3). The amount and size of the clusters is quantified using Ripley's K-function analysis (Fig. 1d). The integrated areas of the Ripley's K-function curves indicate there are more RAGE clusters compared to $RAGE_{RQ/AA}$ clusters. In addition, RAGE has clusters as large as 760 nm, however, $RAGE_{RQ/AA}$ does not exhibit clusters larger than 610 nm (i.e., there is a random distribution over a longer length scale). This shows that altering the interaction between RAGE and Diaph1 also alters the amount and size of RAGE clusters in HEK 293 cells. A previously reported NMR structural analysis showed that increasing the molecular dimension of RAGE resulted in recruiting Diaph1 and initiating signal transduction [21]. When Diaph1 is not recruited due to altering the interaction between Diaph1 and RAGE, both RAGE clustering and its associated signal transduction pathways may be altered.

The influence of Diaph1 on RAGE clusters was further analyzed in a cell line with reduced Diaph1 expression (RAGE-Diaph1$^{-/-}$). The concentration of Diaph1 is reduced, but not eliminated in these experiments, as shown in Fig. S2c and Fig. S2d. Diaph1 is a formin family protein, and is known to affect the formation of actin filaments [28]. In order to confirm the reduced levels of Diaph1 achieved in this study had a similar effect on the actin cytoskeleton as previously reported, phalloidin staining of the actin cytoskeleton was measured (Fig. 2a). As shown in Fig.2b-2c, the filopodia density (0.24 ± 0.05 μm^{-1}) and length (2.1 ± 0.2 μm) increase in cells expressing RAGE when compared to wild-type HEK 293 cells that do not express exogenous RAGE. This is consistent with previous reports [54]. The filopodia density and length decrease by 61% and 37%, respectively, in RAGE-Diaph1$^{-/-}$ cells compared with cells expressing both RAGE and Diaph1. After Diaph1 expression is reduced, the values are statistically the same as those measured for cells that do not express transgenic RAGE, indicating that the increased filopodia length and density resulting from RAGE expression can be eliminated by reducing the expression of Diaph1. In $RAGE_{RQ/AA}$ cells, the filopodia density increased, although the filopodia length is not significantly different compared to cells expressing RAGE. This indicates that alterations to the actin cytoskeleton also occur in the cell line where the interaction between Diaph1 and RAGE is blocked, although the alterations are not as pronounced as when Diaph1 expression is reduced.

Fewer RAGE clusters are measured in the RAGE-Diaph1$^{-/-}$ cell line compared to cells expressing native Diaph1 levels (Figure 1d), which is consistent with the data for cells expressing $RAGE_{RQ/AA}$. The RAGE-Diaph1$^{-/-}$ cell line, however, exhibits a larger amount of smaller clusters. Also, the largest cluster size is 510 nm in the RAGE-Diaph1$^{-/-}$ cell line, which is smaller than the value for $RAGE_{RQ/AA}$. Reducing the concentration of Diaph1 and

disrupting its interaction with RAGE produce both fewer and smaller RAGE clusters compared to the control cell line, but there may be distinct mechanisms for how the RAGE clusters are altered in these cell lines.

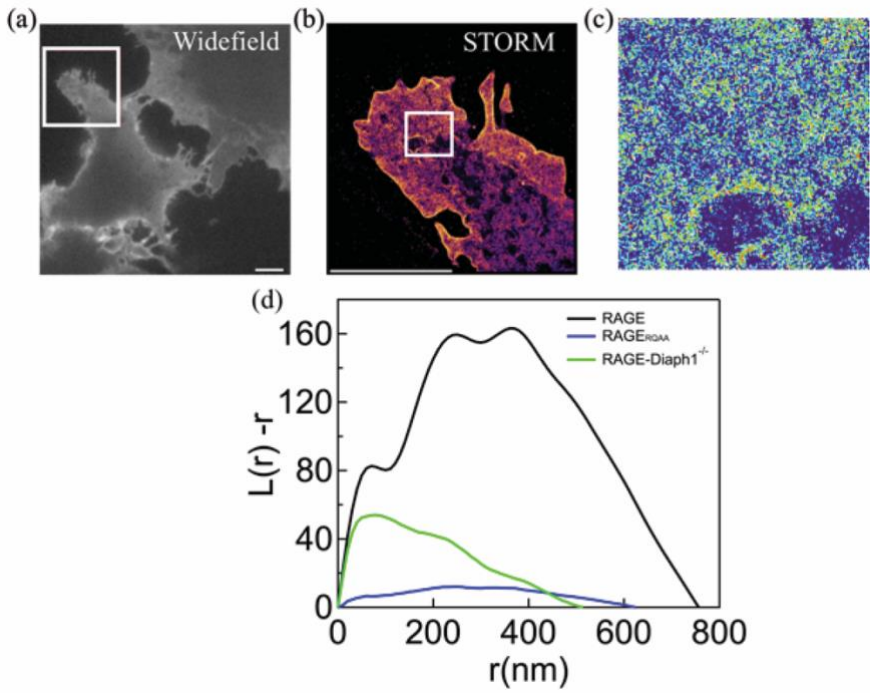

Figure 1. RAGE spatial organization in the plasma membrane of HEK 293 cells as measured by fluorescence microscopy. (a) Wide-field diffraction-limited image measured by primary anti-RAGE antibody with Alexa Fluor 647 F(ab')2-Goat anti-rabbit secondary antibody. The white box represents the region where STORM measurements were performed. The scale bar is 10 μm. (b) Reconstructed STORM image. The white box represents the region where cluster analysis was performed. Scale bar is 10 μm. (c) Heat map showing the results from cluster analysis of a (4 μm × 4 μm) region. The color indicates the degree of clustering from low (dark blue) to high (red). (d) Plots of Ripley's K-function analysis of the clustering properties of RAGE, $RAGE_{RQ/AA}$, RAGE-Diaph1$^{-/-}$ in HEK293 cells (n = 4 for each cell type). L(r)-r represents the clustering ability, and r represents the radial clustering scale.

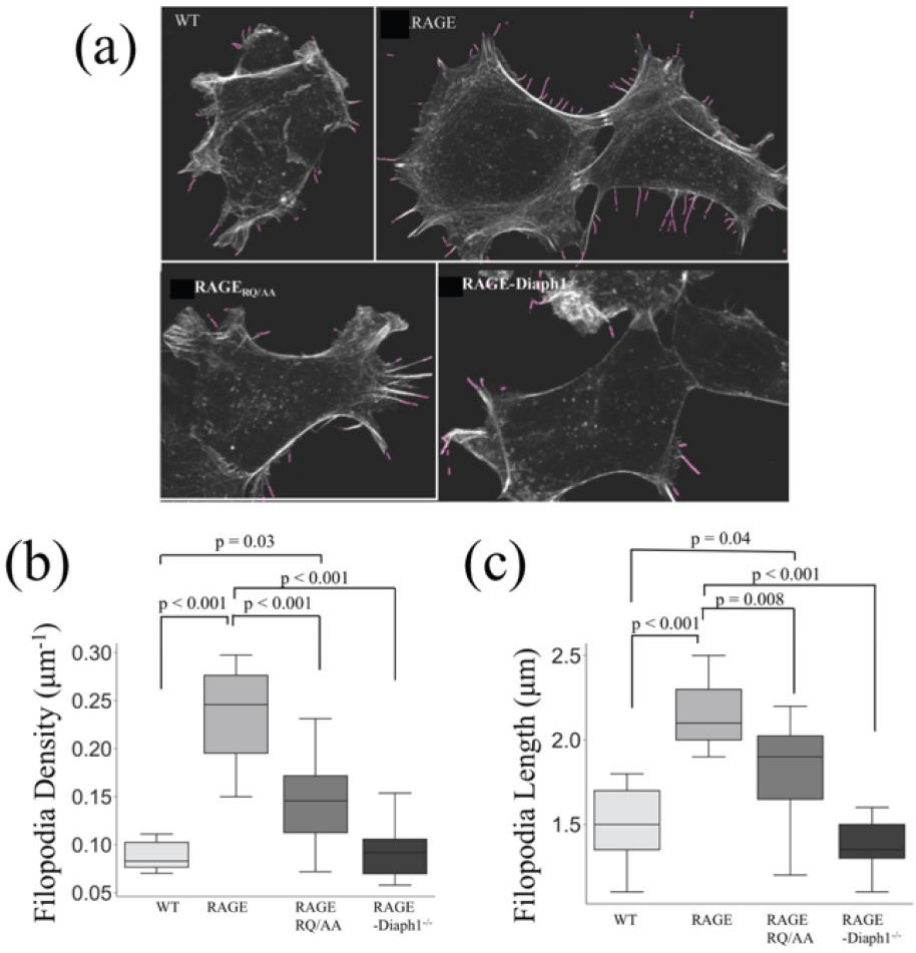

Figure 2. Filopodia density and length measured when the actin cytoskeleton is stained with Atto 647N-conjugated phalloidin in HEK 293 cells. The number of analyzed cells are: wild-type (WT) HEK293 cell line (n = 8), cells expressing RAGE (n = 10), cells expressing RAGE$_{RQ/AA}$ (n = 13), RAGE-Diaph1$^{-/-}$ cells (n = 15). (a) The filopodia detected using FiloQuant are labeled with a pink line in each image. Box plots of (b) the filopodia density and (c) filopodia length. The line inside the box represents the mean value. The box shows the twenty-fifth and seventy-fifth quartiles with the mean shown within the box. The thin line is 1.5 times the interquartile range. p-values are obtained from Student's t-test with a two-tailed distribution (parametric distribution).

3.2 RAGE diffusion in HEK 293 cells is altered differently when Diaph1 expression is reduced compared to when the Diaph1 binding site is altered

RAGE diffusion was measured in HEK 293 cells using SPT. First a cumulative probability distribution (CPD) analysis of the trajectories was performed to determine the number of diffusing populations that could be measured as well as the diffusion coefficient of each population. Next the properties of transient confinement within each trajectory were

measured to obtain the diffusion coefficient and residence time in confined domains as well as the sized of the confined domains.

As shown in Fig. 3a-3b, RAGE diffusion (i.e., mean square displacement versus probability plot) is better fit by a model with two populations (2p model) than a model with one population (1p model). The two populations will be referred to as the fast fraction and slow fraction. The diffusion coefficient for each population can be obtained from a fit to the MSD versus time plot (Fig.3d-3e). There is no statistically significant difference between the fit for Brownian diffusion and anomalous motion for either the fast or the slow population, thus the simpler Brownian fit was used to quantify the diffusion coefficients. The RAGE diffusion coefficients for the fast (D_f) and slow (D_s) population are 0.107 $\mu m^2/s$ and 0.0149 $\mu m^2/s$, respectively. A 72% majority of the RAGE exhibits fast diffusion (Fig.3c).

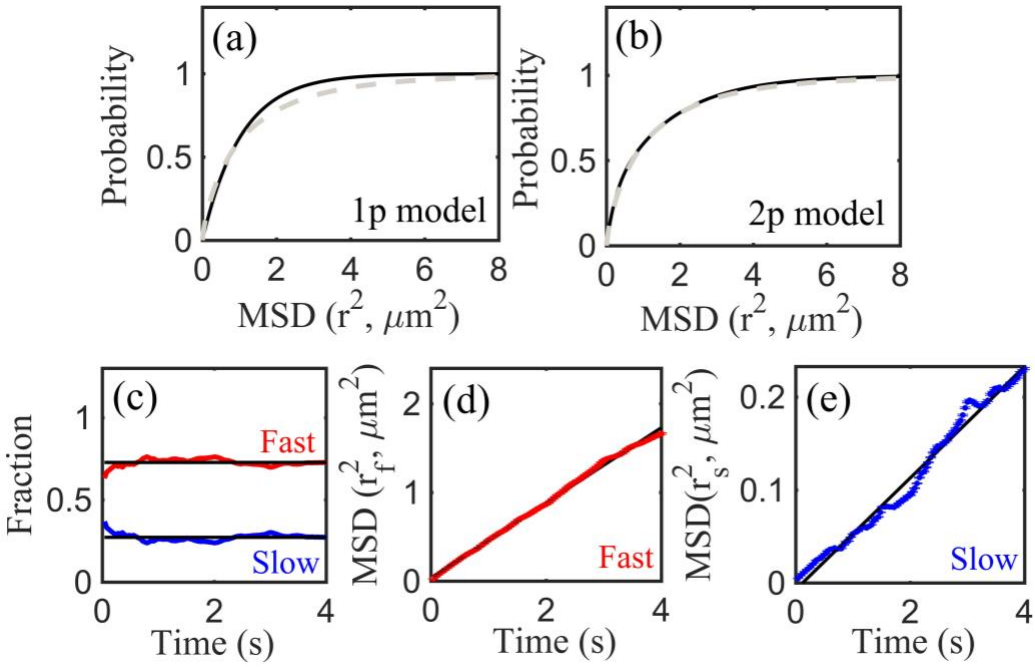

Figure 3. RAGE diffusion properties obtained from all trajectories (n = 130) measured in HEK 293 cells. The average of all trajectories' cumulative probability distribution (CPD) with a 4 sec lag time versus squared step sizes (r^2) are fit using (a) single population model (1p) and (b) two population model (2p). The grey dashed line represents the CPD, the solid black line represents the fit curve. (c) Fractions of the fast population and slow population calculated using the 2p model. The average MSD

plots for the (d) fast and (e) slow population versus lag time. The black line represents fit curves.

The cumulative probability distribution curve for $RAGE_{RQ/AA}$ and RAGE-Diaph1$^{-/-}$ is also best described using a 2 population model (Fig. S4a-4b, Fig. S5a-5b). All fit results are summarized in Fig. 4. Both the fast and slow diffusion coefficient for $RAGE_{RQ/AA}$ show a statistically significant decrease to 0.094 $\mu m^2/s$ and 0.011$\mu m^2/s$, respectively, compared with the diffusion coefficients for RAGE (Fig.4b-Fig.4c). The interaction between RAGE and Diaph1 increases RAGE diffusion, which is slower when the RAGE/Diaph1 interaction is blocked at the known binding site on RAGE.

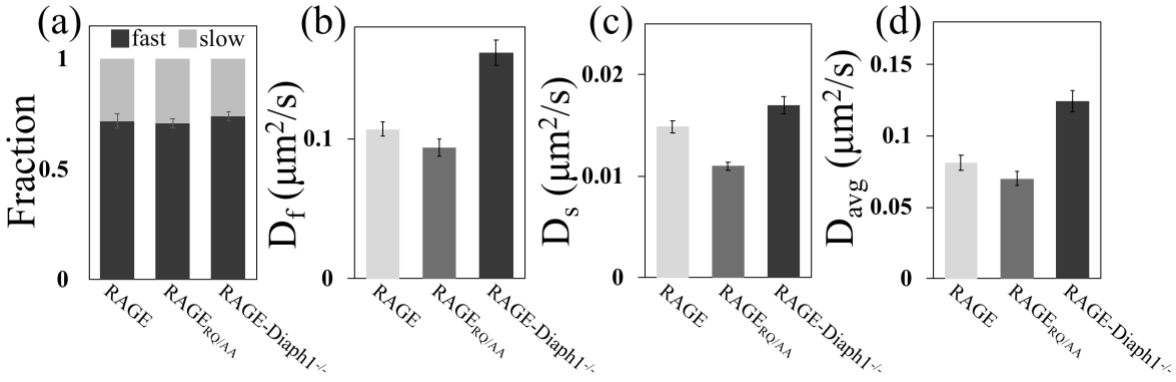

Figure 4. Average diffusion properties of RAGE (n = 145), $RAGE_{RQ/AA}$ (n = 185), RAGE-Diaph1$^{-/-}$ (n = 131) in HEK 293 cells. (a) Fraction of the total RAGE exhibiting both fast diffusion and slow diffusion, and the diffusion coefficient for (b) the fast population (D_f) and (c) the slow population (D_s) obtained from a double exponential fit to the cumulative probability distributions. (d) Average diffusion coefficient for the sum of both D_f and D_s multiplied by their individual fraction. The error bars represent the standard error in the fit.

When Diaph1 expression is reduced, there is an increase in the fast diffusion coefficient for RAGE to 0.162 $\mu m^2/s$ (Fig 4b), which may be the result of disrupting the protein interaction (or possibly a protein complex) or it may be the result of the altered cytoskeleton (Fig. 2). In a previous study, we showed the RAGE diffusion coefficient decreased by 37 % when actin

filament depolymerization is inhibited by treatment with jasplakinolide in GM07373 cells [36]. Considering this previous finding, it is not surprising to measure a 35 % increase in the average RAGE diffusion coefficient when actin polymerization is reduced by the lower expression levels of Diaph1. It is proposed that the population of RAGE with a faster diffusion coefficient is impacted by the structure of the actin cytoskeleton, which is why this population has a faster diffusion coefficient when Diaph1 expression is reduced.

RAGE diffusion exhibits transient events that represent diffusion within confined domains (Fig.S6). Additional information about RAGE diffusion within confined domains can be obtained from analyzing the local displacement of segments of each trajectory. The average diffusion coefficient of RAGE in confined domains (D_{in}) is 0.018 $\mu m^2/s$ (Fig. 5a). The average diffusion coefficient of $RAGE_{RQ/AA}$ within confined domains is statistically lower (0.013 $\mu m^2/s$). Both the magnitude of the diffusion coefficient as well as the relative decrease when comparing the diffusion coefficients for RAGE and $RAGE_{RQ/AA}$ suggest that the slow population from the CPD analysis may represent those receptors that are diffusing within confined domains. Coincident with the decrease in the diffusion coefficient for $RAGE_{RQ/AA}$ in confined domains, there is also a decrease in the size of the confined domains (0.18 μm) compared to RAGE (0.23 μm) (Fig. 5b). For all other cellular conditions, the differences in the diffusion coefficient and size of confined domains were not statistically significant ($p > 0.02$). (Fig. 5c).

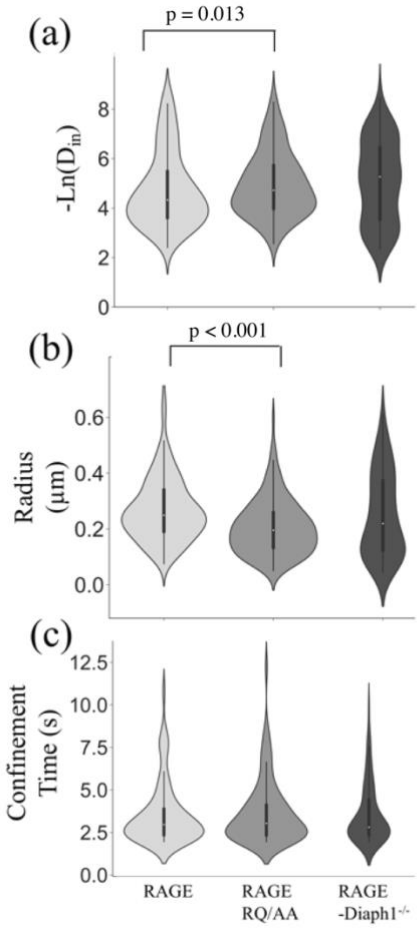

Figure 5. Analysis of all the trajectories exhibiting confined motion in HEK 293 cells. The number of analyzed confined domains are RAGE (n = 140), $RAGE_{RQ/AA}$ (n = 182), RAGE-Diaph1$^{-/-}$ (n = 91). Violin plot of the (a) negative natural log of the diffusion coefficients within confined domains, (b) size of confined domains, and (c) duration of time in confined domains. The width of violin plot represents the data distribution. Overlapping each violin plot is a box plot showing the mean (white dot) of all values within the data set. The solid line shows the twenty-fifth and seventy-fifth quartiles. The thin line is 1.5 times the interquartile range. p-values were obtained from the Mann-Whitney test (non-parametric distribution).

4. Conclusions and future insights

Diaph1 affects RAGE clusters and RAGE's diffusion properties. Reducing the expression of Diaph1 and eliminating the binding site to RAGE have similar effects on reducing the size and number of RAGE clusters, but do not have the same effects on RAGE diffusion. Decreased RAGE diffusion is only measured when the known site of interaction with Diaph1 is altered on the RAGE cytoplasmic tail. Both the fast and slow populations are affected, and

the changes to the slow population may correlate with alterations to properties of confined domains in the membrane. Reducing the expression of Diaph1 increases RAGE diffusion; the mechanism is proposed to involve the concomitant changes to actin polymerization. This shows that Diaph1 can affect RAGE diffusion and clusters, and that these properties are influenced by the intracellular environment.

Author contributions

Q.Z. and E.A.S. designed the research, analyzed the results, and wrote the manuscript. Q.Z. developed the cell lines used in this study and performed the experiments.

Acknowledgements

This work was initiated with funding from NSF grant CHE-1412084 and was continued with funding from NSF grant CHE-1709099. The authors thank Dr. Aleem Syed for useful discussion and help with protein cloning.

References

[1] M. Neeper, A.M. Schmidt, J. Brett, S.D. Yan, F. Wang, Y.C. Pan, K. Elliston, D. Stern, A. Shaw, Cloning and expression of a cell surface receptor for advanced glycosylation end products of proteins, *J Biol Chem*, 267 (1992) 14998-15004.
[2] A.M. Schmidt, M. Vianna, M. Gerlach, J. Brett, J. Ryan, J. Kao, C. Esposito, H. Hegarty, W. Hurley, M. Clauss, et al., Isolation and characterization of two binding proteins for advanced glycosylation end products from bovine lung which are present on the endothelial cell surface, *J Biol Chem*, 267 (1992) 14987-14997.
[3] A.M. Schmidt, M. Hasu, D. Popov, J.H. Zhang, J.X. Chen, S.D. Yan, J. Brett, R. Cao, K. Kuwabara, G. Costache, N. Simionescu, M. Simionescu, D. Stern, Receptor for Advanced Glycation End-Products (Ages) Has a Central Role in-Vessel Wall Interactions and Gene Activation in Response to Circulating Age Proteins, *P Natl Acad Sci USA*, 91 (1994) 8807-8811.
[4] M.A. Hofmann, S. Drury, C. Fu, W. Qu, A. Taguchi, Y. Lu, C. Avila, N. Kambham, A. Bierhaus, P. Nawroth, M.F. Neurath, T. Slattery, D. Beach, J. McClary, M. Nagashima, J. Morser, D. Stern, A.M. Schmidt, RAGE mediates a novel proinflammatory axis: a central cell surface receptor for S100/calgranulin polypeptides, *Cell*, 97 (1999) 889-901.
[5] J.K. Juranek, G.K. Daffu, J. Wojtkiewicz, D. Lacomis, J. Kofler, A.M. Schmidt, Receptor for Advanced Glycation End Products and its Inflammatory Ligands are Upregulated in Amyotrophic Lateral Sclerosis, *Front Cell Neurosci*, 9 (2015) 485.
[6] T. Ostendorp, E. Leclerc, A. Galichet, M. Koch, N. Demling, B. Weigle, C.W. Heizmann, P.M.H. Kroneck, G. Fritz, Structural and functional insights into RAGE activation by multimeric S100B, *Embo Journal*, 26 (2007) 3868-3878.
[7] J.R. Klune, R. Dhupar, J. Cardinal, T.R. Billiar, A. Tsung, HMGB1: endogenous danger signaling, *Mol Med*, 14 (2008) 476-484.
[8] S.D. Yan, H. Zhu, A. Zhu, A. Golabek, H. Du, A. Roher, J. Yu, C. Soto, A.M. Schmidt, D. Stern, M. Kindy, Receptor-dependent cell stress and amyloid accumulation in systemic amyloidosis, *Nat Med*, 6 (2000) 643-651.
[9] R. Deane, S. Du Yan, R.K. Submamaryan, B. LaRue, S. Jovanovic, E. Hogg, D. Welch, L. Manness, C. Lin, J. Yu, H. Zhu, J. Ghiso, B. Frangione, A. Stern, A.M. Schmidt, D.L. Armstrong, B. Arnold, B. Liliensiek, P. Nawroth, F. Hofman, M. Kindy, D. Stern, B. Zlokovic, RAGE mediates amyloid-beta peptide transport across the blood-brain barrier and accumulation in brain, *Nat Med*, 9 (2003) 907-913.
[10] T. Chavakis, A. Bierhaus, N. Al-Fakhri, D. Schneider, S. Witte, T. Linn, M. Nagashima, J. Morser, B. Arnold, K.T. Preissner, P.P. Nawroth, The pattern recognition receptor (RAGE) is a counterreceptor for leukocyte integrins: A novel pathway for inflammatory cell recruitment, *J Exp Med*, 198 (2003) 1507-1515.
[11] J. Juranek, R. Ray, M. Banach, V. Rai, Receptor for advanced glycation end-products in neurodegenerative diseases, *Rev Neurosci*, 26 (2015) 691-698.
[12] J. Li, A.M. Schmidt, Characterization and functional analysis of the promoter of RAGE, the receptor for advanced glycation end products, *J Biol Chem*, 272 (1997) 16498-16506.
[13] E.J. Lee, J.H. Park, Receptor for Advanced Glycation Endproducts (RAGE), Its Ligands, and Soluble RAGE: Potential Biomarkers for Diagnosis and Therapeutic Targets for Human Renal Diseases, *Genomics Inform*, 11 (2013) 224-229.
[14] J. Xie, S. Reverdatto, A. Frolov, R. Hoffmann, D.S. Burz, A. Shekhtman, Structural basis for pattern recognition by the receptor for advanced glycation end products (RAGE), *J Biol Chem*, 283 (2008) 27255-27269.
[15] L. Yatime, G.R. Andersen, Structural insights into the oligomerization mode of the human receptor for advanced glycation end-products, *Febs J*, 280 (2013) 6556-6568.

[16] H.J. Huttunen, C. Fages, H. Rauvala, Receptor for advanced glycation end products (RAGE)-mediated neurite outgrowth and activation of NF-kappaB require the cytoplasmic domain of the receptor but different downstream signaling pathways, *J Biol Chem*, 274 (1999) 19919-19924.
[17] R. Bianchi, E. Kastrisianaki, I. Giambanco, R. Donato, S100B protein stimulates microglia migration via RAGE-dependent up-regulation of chemokine expression and release., *The Journal of biological chemistry*, 286 (2011) 7214-7226.
[18] A. Rouhiainen, J. Kuja-Panula, S. Tumova, H. Rauvala, RAGE-mediated cell signaling, *Methods Mol Biol*, 963 (2013) 239-263.
[19] H.L. Zong, A. Madden, M. Ward, M.H. Mooney, C.T. Elliott, A.W. Stitt, Homodimerization Is Essential for the Receptor for Advanced Glycation End Products (RAGE)-mediated Signal Transduction, *Journal of Biological Chemistry*, 285 (2010) 23135-23144.
[20] K. Ishihara, K. Tsutsumi, S. Kawane, M. Nakajima, T. Kasaoka, The receptor for advanced glycation end-products (RAGE) directly binds to ERK by a D-domain-like docking site, *FEBS Lett*, 550 (2003) 107-113.
[21] J. Xue, M. Manigrasso, M. Scalabrin, V. Rai, S. Reverdatto, D.S. Burz, D. Fabris, A.M. Schmidt, A. Shekhtman, Change in the Molecular Dimension of a RAGE-Ligand Complex Triggers RAGE Signaling, *Structure*, 24 (2016) 1509-1522.
[22] B.I. Hudson, A.Z. Kalea, M.D. Arriero, E. Harja, E. Boulanger, V. D'Agati, A.M. Schmidt, Interaction of the RAGE Cytoplasmic Domain with Diaphanous-1 Is Required for Ligand-stimulated Cellular Migration through Activation of Rac1 and Cdc42, *Journal of Biological Chemistry*, 283 (2008) 34457-34468.
[23] Y. Xu, F. Toure, W. Qu, L. Lin, F. Song, X. Shen, R. Rosario, J. Garcia, A.M. Schmidt, S.F. Yan, Advanced glycation end product (AGE)-receptor for AGE (RAGE) signaling and up-regulation of Egr-1 in hypoxic macrophages, *J Biol Chem*, 285 (2010) 23233-23240.
[24] A. Shekhtman, R. Ramasamy, A.M. Schmidt, Glycation & the RAGE axis: targeting signal transduction through DIAPH1, *Expert Review of Proteomics*, 14 (2017) 147-156.
[25] V. Rai, A.Y. Maldonado, D.S. Burz, S. Reverdatto, S.F. Yan, A.M. Schmidt, A. Shekhtman, Signal transduction in receptor for advanced glycation end products (RAGE): solution structure of C-terminal rage (ctRAGE) and its binding to mDia1, *J Biol Chem*, 287 (2012) 5133-5144.
[26] F. Toure, G. Fritz, Q. Li, V. Rai, G. Daffu, Y.S. Zou, R. Rosario, R. Ramasamy, A.S. Alberts, S.F. Yan, A.M. Schmidt, Formin mDia1 mediates vascular remodeling via integration of oxidative and signal transduction pathways, *Circ Res*, 110 (2012) 1279-1293.
[27] B.R. Acharya, S.K. Wu, Z.Z. Lieu, R.G. Parton, S.W. Grill, A.D. Bershadsky, G.A. Gomez, A.S. Yap, Mammalian Diaphanous 1 Mediates a Pathway for E-cadherin to Stabilize Epithelial Barriers through Junctional Contractility, *Cell Rep*, 18 (2017) 2854-2867.
[28] C. Higashida, T. Miyoshi, A. Fujita, F. Oceguera-Yanez, J. Monypenny, Y. Andou, S. Narumiya, N. Watanabe, Actin polymerization-driven molecular movement of mDia1 in living cells, *Science*, 303 (2004) 2007-2010.
[29] A.F. Palazzo, T.A. Cook, A.S. Alberts, G.G. Gundersen, mDia mediates Rho-regulated formation and orientation of stable microtubules, *Nat Cell Biol*, 3 (2001) 723-729.
[30] S. Narumiya, M. Tanji, T. Ishizaki, Rho signaling, ROCK and mDia1, in transformation, metastasis and invasion, *Cancer Metastasis Rev*, 28 (2009) 65-76.
[31] H. Mellor, The role of formins in filopodia formation, *Biochim Biophys Acta*, 1803 (2010) 191-200.
[32] Y.N. Lin, R. Bhuwania, K. Gromova, A.V. Failla, T. Lange, K. Riecken, S. Linder, M. Kneussel, J.R. Izbicki, S. Windhorst, Drosophila homologue of Diaphanous 1 (DIAPH1)

controls the metastatic potential of colon cancer cells by regulating microtubule-dependent adhesion, *Oncotarget*, 6 (2015) 18577-18589.
[33] R.J. Cherry, Rotational and lateral diffusion of membrane proteins, *Biochim Biophys Acta*, 559 (1979) 289-327.
[34] S. Ramadurai, A. Holt, V. Krasnikov, G. van den Bogaart, J.A. Killian, B. Poolman, Lateral diffusion of membrane proteins, *J Am Chem Soc*, 131 (2009) 12650-12656.
[35] P.A. Liebman, A historical perspective on the lateral diffusion model of GTPase activation and related coupling of membrane signaling proteins, *Cell Logist*, 4 (2014) e29389.
[36] A. Syed, Q. Zhu, E.A. Smith, Lateral diffusion and signaling of receptor for advanced glycation end-products (RAGE): a receptor involved in chronic inflammation, *Eur Biophys J*, (2017).
[37] G. Jacquemet, I. Paatero, A.F. Carisey, A. Padzik, J.S. Orange, H. Hamidi, J. Ivaska, FiloQuant reveals increased filopodia density during breast cancer progression, *J Cell Biol*, 216 (2017) 3387-3403.
[38] C.A. Schneider, W.S. Rasband, K.W. Eliceiri, NIH Image to ImageJ: 25 years of image analysis, *Nat Methods*, 9 (2012) 671-675.
[39] M. Ovesny, P. Krizek, J. Borkovec, Z. Svindrych, G.M. Hagen, ThunderSTORM: a comprehensive ImageJ plug-in for PALM and STORM data analysis and super-resolution imaging, *Bioinformatics*, 30 (2014) 2389-2390.
[40] S. Malkusch, M. Heilemann, Extracting quantitative information from single-molecule super-resolution imaging data with LAMA - LocAlization Microscopy Analyzer, *Sci Rep*, 6 (2016) 34486.
[41] A. Syed, Q. Zhu, E.A. Smith, Ligand binding affinity and changes in the lateral diffusion of receptor for advanced glycation endproducts (RAGE), *Biochim Biophys Acta*, 1858 (2016) 3141-3149.
[42] D. Mainali, E.A. Smith, Select cytoplasmic and membrane proteins increase the percentage of immobile integrins but do not affect the average diffusion coefficient of mobile integrins, *Anal Bioanal Chem*, 405 (2013) 8561-8568.
[43] I.F. Sbalzarini, P. Koumoutsakos, Feature point tracking and trajectory analysis for video imaging in cell biology, *J Struct Biol*, 151 (2005) 182-195.
[44] G.J. Schutz, H. Schindler, T. Schmidt, Single-molecule microscopy on model membranes reveals anomalous diffusion, *Biophys J*, 73 (1997) 1073-1080.
[45] A. Matysik, R.S. Kraut, TrackArt: the user friendly interface for single molecule tracking data analysis and simulation applied to complex diffusion in mica supported lipid bilayers, *BMC Res Notes*, 7 (2014) 274.
[46] L. Niu, J. Yu, Investigating intracellular dynamics of FtsZ cytoskeleton with photoactivation single-molecule tracking, *Biophys J*, 95 (2008) 2009-2016.
[47] T.Y. Chen, A.G. Santiago, W. Jung, L. Krzeminski, F. Yang, D.J. Martell, J.D. Helmann, P. Chen, Concentration- and chromosome-organization-dependent regulator unbinding from DNA for transcription regulation in living cells, *Nat Commun*, 6 (2015) 7445.
[48] J.C. Gebhardt, D.M. Suter, R. Roy, Z.W. Zhao, A.R. Chapman, S. Basu, T. Maniatis, X.S. Xie, Single-molecule imaging of transcription factor binding to DNA in live mammalian cells, *Nat Methods*, 10 (2013) 421-426.
[49] S. Uphoff, R. Reyes-Lamothe, F. Garza de Leon, D.J. Sherratt, A.N. Kapanidis, Single-molecule DNA repair in live bacteria, *Proc Natl Acad Sci U S A*, 110 (2013) 8063-8068.
[50] M.A. Deverall, E. Gindl, E.K. Sinner, H. Besir, J. Ruehe, M.J. Saxton, C.A. Naumann, Membrane lateral mobility obstructed by polymer-tethered lipids studied at the single molecule level, *Biophys J*, 88 (2005) 1875-1886.

[51] R. Simson, E.D. Sheets, K. Jacobson, Detection of Temporary Lateral Confinement of Membrane-Proteins Using Single-Particle Tracking Analysis, *Biophysical Journal*, 69 (1995) 989-993.
[52] S.A. Menchon, M.G. Martin, C.G. Dotti, APM_GUI: analyzing particle movement on the cell membrane and determining confinement, *Bmc Biophysics*, 5 (2012).
[53] P.J. Bosch, J.S. Kanger, V. Subramaniam, Classification of dynamical diffusion states in single molecule tracking microscopy, *Biophys J*, 107 (2014) 588-598.
[54] F. Xiong, S. Leonov, A.C. Howard, S. Xiong, B. Zhang, L. Mei, P. McNeil, S. Simon, W.C. Xiong, Receptor for advanced glycation end products (RAGE) prevents endothelial cell membrane resealing and regulates F-actin remodeling in a beta-catenin-dependent manner, *J Biol Chem*, 286 (2011) 35061-35070.